THE MODEL FOR HELICAL SHELLS TESTING

Sreten Savićević, Željko Ivandić, Janko Jovanović, Luka Grubiša, Antun Stoić, Milan Vukčević, Mileta Janjić

In this paper we present a model for the experimental and numerical study of helical shells. Three different forms were chosen for the experiment: Model A forms a helicoidal shell on a cylindrical shell, Model B is an annular shell on a cylindrical shell and Model C a rectangular plate on a cylindrical shell.. Placing a continuous load on the surface of the shell was achieved by normal pressure, thanks to special sealing elements within the construction of the double helical shell.The strain was measured using strain gauges. Comparable results were obtained using the ANSYS Workbench software package for analysis using the finite element method. The experimental investigation confirmed that the numerical modelling provides relevant results for the stress, deformation and deflections of continuously loaded helical shells.

Keywords: displacement; FEA; helicoidal shell; radial stress

Model ispitivanja helikoidalnih ljuski

U radu su predstavljeni modeli za eksperimentalno i numeričko istraživanje zavojne ljuske. Tri oblika su odabrana za eksperiment: model A predstavlja zavojnu ljusku na cilindričnoj ljuski, model B kružnu ljusku na cilindričnoj ljuski, i model C pravokutnu ljusku na cilindričnoj ljusci. Ostvarenje kontinualnog opterećenja po površini ljuske je izvršeno pomoću normalnog tlaka koga osigurava konstrukcija sa dvostrukom zavojnom ljuskom sa posebnim elementima za brtvljenje. Mjerenje naprezanja je izvršeno korištenjem mjernih traka. Usporedni rezultati su dobiveni uporabom softverskog paketa za analizu pomoću metode konačnih elemenata ANSYS Workbench. Eksperimentalna istraživanja su potvrdila da numeričko modeliranje daje mjerodavne rezultate naprezanja, deformacija i ugiba kontinualno opterećene zavojne ljuske.

Ključne riječi: MKE; pomaci; radijalna naprezanja; zavojna ljuska

1   Introduction

The working parts of the helicoidal shell shape are applied to devices of continual transport, helicoidal transporters, in specialized snow blowing machines, and so forth. The helicoidal shell for these devices is usually made by forging it from sheet-steel or strap-steel using specialized machines, and then welding them to a rotary part. In helicoidal transporters, this shell is welded to the shaft or pipe; whereas in the snow blowing machines and in ones that are similar, this shell is welded to thin cylindrical shells of a larger diameter. The analytical methods to calculate the dimensions of the loaded plates and shells are well known in the mechanics of a deformable body. A few geometrically simple parts in the shape of plates and shells have been analyzed using these methods.

Despite a number of scientists who have investigated the shells, only a few of them worked on the helicoidal shells. A significant contribution in this field has been made by: A. L. Goldenveizer [1], T. S. Timoshenko [2], P. M. Naghdi [3], V. I. Feodoseev, [4], W. S. Wlassow [5], V. V. Novozhilov [6], S. N. Krivoshapko [7,8], T. Merlini [9].

A few papers dealing with shell bending have been published, and they have only addressed theoretical analyses. Any application of shell theory equations, and their solutions, in the case of the helicoidal shell is extremely complex. Some papers addressing this problem have been published, including those by J. W. Cohen [10, 11] and S. G. Mikhlin [12]. J.W. Cohen developed the relation between strains and displacements by comparing the relevant geometric features (lengths, angles, and curvatures) in deformed and non-deformed structures. He derived the differential equations of equilibrium by analyzing the equilibrium of an infinitesimal element of the shell, while the coordinate axes do not follow the curvature lines. These equations are in agreement with the differential equations derived using the law of momentum conservation the restricted theory of shells. The constitutive equations that relate the strain parameters to the stress parameters given by Cohen [9] were not obtained using the principle of a minimum deformation of work for shells, something that is widely used in the restricted theory of shells. Therefore, the equations obtained using these two methods are different. Conversely, the ordinary Love's constitutive equations were used by S. G. Mikhlin [13] in his work. In a paper [18], they give an original analytical model for the determination of the voltage deformation parameters of helicoidal shells.

In this paper, we present a numerical analysis of the parameters of the continuous load of a helicoidal shell, verified by experimental investigation. The numerical analysis was conducted using the method of finite elements, employing the ANSYS Workbench software package.

2   Model description for experimental investigation
2.1   Helicoidal shell shape

A helicoidal shell shape is a part of the conoidal helicoidal surface that is connected to a cylindrical shell along its helical line (Fig. 1a). In this case, the conoidal helicoid is generated by a straight line passing through the z-axis as a directrix, parallel to the *Oxy* plane as the directory one, and passing through a helical line as the leading one. The equation for this surface is [14]:

$$z = \frac{H}{2\pi}\arctan\left(\frac{y}{x}\right) \qquad (1)$$

where H is the pace of the helical line. In special cases, when the helical line pace $H=0$, the helicoid becomes a circle; whereby the conoidal helicoid is represented by the *Oxy* plane. If we observe a part of that plane as a ring on a cylindrical shell, we have a special case of a ring-like plate on the cylindrical shell. If the helical line pace $H=\infty$, then the helical line turns into a straight line parallel to the *Oz* axis. Then, it becomes a special case of a rectangular plate attached to the cylindrical shell that is perpendicular to the *Oxy* plane.

On the basis of theoretical analysis [18], three models were chosen for the experimental investigation:

1) The first was for an analysis of the step coils, which can range from 0 to ∞, i.e..: $0 \leq H \leq \infty$. Model *A* represents a helicoidal shell stiffly fixed on a cylindrical shell along the helical line with a constant pace of $H=140$ mm (Fig. 1a).

2) Model *B* represents an annular shell stiffly fixed on the cylindrical shell (Fig. 1b). This model is a special case of the helicoidal shell with a pace of $H=0$.

3) Model *C* represents a rectangular shell stiffly fixed on the cylindrical shell (Fig. 1c). This model is a special case of the helicoidal shell with a pace of $H=\infty$.

These models were conceived after analyzing the possibilities of fabricating a helicoidal shell as a geometrical complex machine element. It is not possible to derive precise deformation analyses of the models made by welding the segments of the helicoidal shell due to dimension deviations, particularly because of the helicoidal surface inclination. Consequently, it was suggested that the helicoidal shell structure be manufactured by metal cutting in order to obtain a high level of geometrical accuracy that was needed for precise deformation analyses. In addition, a high level of accuracy is necessary to assure the sealing between parts during the loading of the helicoidal shell. The models of annular and rectangular shells were made by welding these shells to the cylindrical shell followed by metal cutting.

The three chosen models, with identical values of both the outer and inner shells, which have the following diameters ($D=400$ mm, $d=260$ mm), height ($h=420$ mm), and thickness ($\delta_1=4$ mm and $\delta_2=6$ mm). Therefore, the obtained experimental results for the helicoidal shell in the whole range of its possible shapes are comparable. At the same time, this uniformity of dimensions allowed the same experimental chamber elements and plates to be used for all the models. The mass of the chosen models being 29 kg for Model A, and 18 kg for Models B and C, allowed manual manipulation and transport without using additional transportation means during the experiment. The ratio between the shell thickness, $\delta_1=4$ mm, and width, $b=70$ mm, is 1:17.5, which meets the necessary criteria and enabled the application of the theory of thin plates and shells to these models.
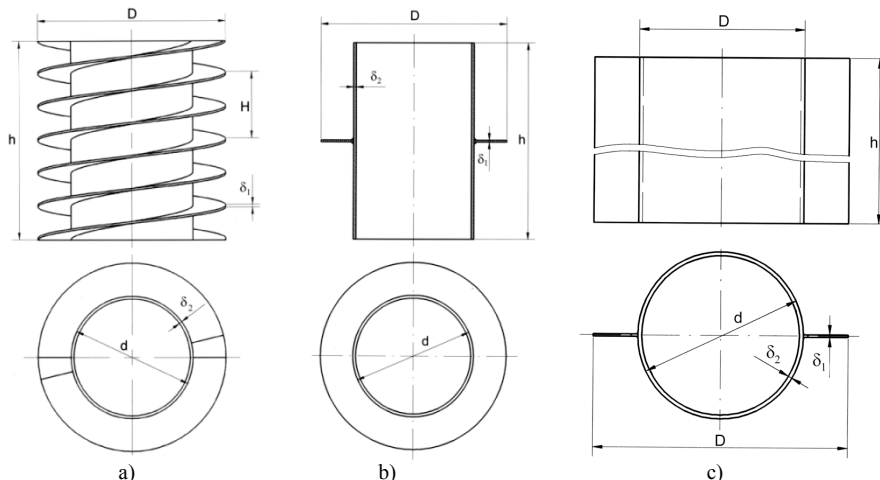

Figure 1 Experimental models: a) Helicoidal shell on a cylindrical shell – Model A, b) Annular shell on a cylindrical shell – Model B, c) Rectangular plate on a cylindrical shell – Model C

2.2 Load on the helicoidal shell

The load acting on the shell may be concentrated, continuous, or combined and of an arbitrary direction. It may have components in the direction of the tangent, the normal, or the binormal. The component in the direction of the binormal represents a component of the helicoidal shell load acting normally with respect to the shell surface that causes its bending. The influence of the continuous load by pressure normally distributed on the helicoidal shell surface on its displacements, strains, and stresses was analyzed in this experimental investigation. The cross-sections of the assemblies for Models A, B, and C, in which the loading of the models was performed by surface pressure are shown in Fig. 2 [15]. One of the major problems at the beginning of planning the experiment was how to load the helicoidal shell by surface pressure. In relation to this, a structure of two helicoidal shells on a cylindrical shell at 180° with respect to each other was suggested (see Fig. 1). In such a double shell structure, air under pressure was introduced into the space between the two shells, so that the shells were exposed to the pressure only from one side. This pressure distribution cannot be achieved with one helicoidal shell structure. In order to seal the space pressurized between the two shells, special rubber sealing elements were glued to the helicoidal shell edges, and the structure was inserted into a chamber. The chamber was closed by two

round plates connected with five long screws to make an assembly as illustrated in Fig. 2. The special seals between the shells and chamber that enable sealing between these elements should, at the same time, enable the displacement of the outer shell edge under the action of normal pressure. The special seal elements were made from an "L" profile rubber strap, with an angle between the sides larger than 90°. Under pressure, these seals adhere to the wall of the cylindrical chamber providing an effective sealing function. To ensure that the special seals simultaneously seal and enable the displacement of the outer edge of the helicoidal shell under pressure, it was necessary to provide a corresponding transition of fits between the shell and the chamber as well as considerable accuracy in assembly parts geometry. In this way, any

collision between the shell and the chamber after assembling was prevented, and the correct results were guaranteed.

Sealing between the round cover plates and the chamber, and the round cover plates and the structure with a double helicoidal shell was performed with round rubber seals inserted into the grooves in the round plates.

The methodology of helicoidal shell sealing by using special rubber seals was applied in sealing the round plates on the cylindrical shell (Fig. 2b), as well as in sealing the two rectangular shells on the cylindrical shell (Fig. 2c). Due to them having the same outer dimensions for each of the testing structures, both the chamber and the round cover plates were used in all three cases.


a)   b)   c)
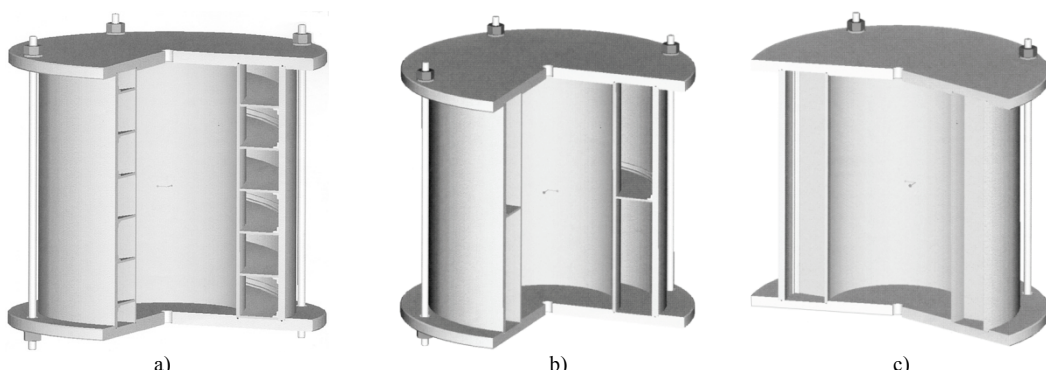
Figure 2 Experimental assembly for Model A, b) Model B, and c) Model C

3 Experimental investigation

The experimental investigation was carried out using a source of pressurized air, and a 60 dm³ capacity compressor operating at a max pressure of 0,8 MPa was used. The shells investigation was carried out at the following values of pressure: 0,05; 0,1; 0,12; 0,14; 0,15; 0,16; 0,18; 0,2; 0,22; 0,24 and 0,25 MPa. A device for precise pressure adjustment was used to regulate the pressure level on the shells. It was installed on the pipe that led air from the compressor to the experimental assembly. A barometer for precise pressure measurement was placed on the chamber. It was designed as a device with a mercury column having an operating range up to 0,25 MPa.

The TDS-303 is an automatic multi-channel data logger for reading 30 strain gauges, which is manufactured by TML - Tokyo Measuring Instruments Laboratory Co., Ltd., Japan. It was used to measure the strain. LY 11 6/120 strain gauges (Hottinger Baldwin Messtechnik GmbH, Germany) were used for the strain measurements. They were attached to the shell structures, after a fine surface preparation, by using two-component glue type P2, manufactured by TML - Tokyo Measuring Instruments Laboratory Co., Ltd., Japan.

Models A, B, and C with the placed and connected strain gauges are shown in Fig. 3, while the complete experimental setup prepared for the investigation is shown in Fig. 4.


a)   b)   c)   d)
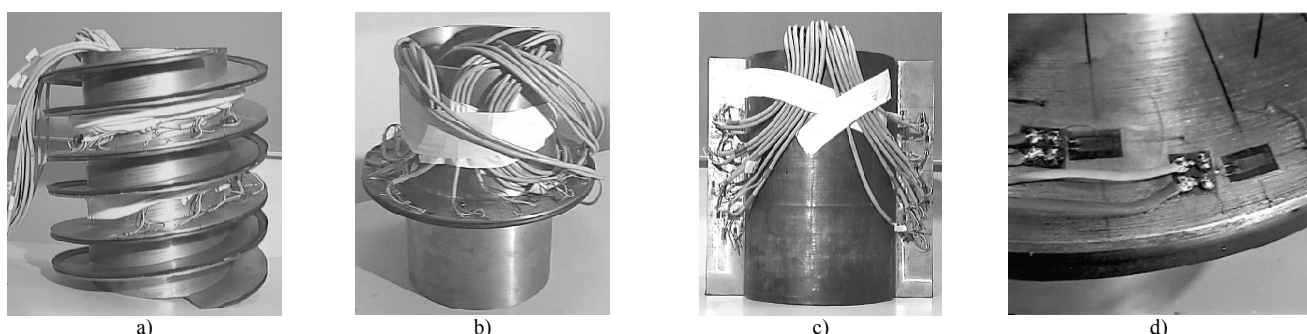
Figure 3 Models prepared for experiment: a) Helicoidal shell on a cylindrical shell – Model A, b) Annular shell on a cylindrical shell – Model B, c) Rectangular shell on a cylindrical shell – Model C, d) Prepared strain gauges

Ninety strain gauges were used for the investigation. Starting from the fact that for the analyzed models the strain value does not depend on the polar coordinate φ but only on the radial coordinate r at the observed point, the

strain measuring was performed in a radial direction, a circular direction, as well as in a direction at an angle of 45° with respect to the radial direction at the two points of the same radius r value. In this way, it was possible to

check the obtained results. A greater concentration of strain gauges was placed in the critical shell zones, close to the edge and to the cylindrical shell, where the values of the circular and radial strains are greater. Thanks to the strain measurement in the three different directions at the points with the same radial coordinate r, it was possible to determine the directions of the principal strain without using classical rosette strain gauges.
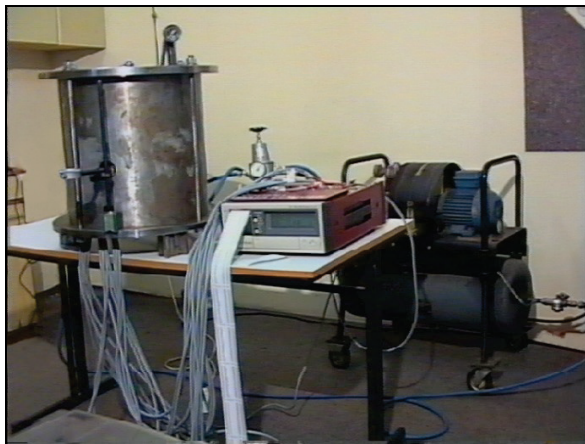
Figure 4 Experimental setup

The material used for Models A, B and C was C45E, according to the EN 10027-1 standard.

4 Experimental results

The experiment was performed at a temperature of 19 °C. The load increased incrementally until it reached 0,25 MPa. Upon reaching each of the preassigned pressure values, the readings from the strain gauges were recorded. After the tensometric investigation was completed, the shell deflection was measured. A device for the deflection measurement was located at the starting point with r=197 mm; from that point, r was varied in the range of 195÷140 mm in increments of 5 mm. The pressure increased incrementally until the predefined values were reached, and the readings of the deflection were recorded.

The strain values ε measured on the steel shell structures during the experimental investigation are presented below. All these strain values represent the bending strains. Membrane shell strains are negligible in these models. Taking into consideration the character of the stress state, the stress values can be calculated using the relations valid for a two-axial stress state:

$$\sigma_1 = E \frac{1}{1-v^2} \left(\varepsilon_1 + v\varepsilon_2 \right) \tag{2}$$

$$\sigma_2 = E \frac{1}{1-v^2} \left(\varepsilon_2 + v\varepsilon_1 \right) \tag{3}$$

A group of the measurement results that represent strain values ε based on the readings from the strain gauges for Models A, B, and C are given in Tabs. 1-3, respectively.

Table 1 Strain ε for Model A

Direction		Radial direction						Circular direction						Direction at angle of 45°			
													Measured strain ×10⁻⁶				
Strain gauge		1	2	3	4	5	6	7	8	9	10	11	12	13	14	15	16
r / mm		140	145	150	170	180	190	140	145	150	170	180	190	145	150	170	180
Pressure p / MPa	0,05	-208	-176	-128	-37	-9	5	-18	-27	-28	-35	-33	-33	-98	-82	-37	-21
	0,1	-406	-343	-247	-70	-18	11	-36	-51	-55	-70	-65	-67	-192	-159	-72	-40
	0,15	-605	-513	-369	-104	-27	17	-55	-76	-82	-106	-98	-102	-287	-239	-108	-63
	0,2	-823	-697	-502	-142	-36	23	-74	-105	-114	-144	-137	-142	-390	-325	-147	-86
	0,25	-1029	-871	-625	-175	-44	29	-93	-129	-141	-182	-172	-180	-487	-404	-183	-108

Table 2. Strain ε for Model B

Direction		Radial direction								Circular direction					Direction at angle of 45°		
														Measured strain ×10⁻⁶			
Strain gauge		1	2	3	4	5	6	7	8	9	10	11	12	13	14	15	16
r / mm		140	145	150	157,5	160	170	180	190	140	145	170	180	190	145	154,5	180
Pressure p / MPa	0,05	-147	-126	-101	-64	-57	-26	-9	3	-6	-16	-24	-24	-21	-65	-51	-15
	0,1	-286	-247	-196	-121	-109	-50	-15	6	-10	-30	-45	-45	-41	-126	-98	-29
	0,15	-432	-371	-296	-182	-164	-75	-23	9	-15	-46	-68	-66	-60	-189	-187	-43
	0,2	-578	-496	-396	-243	-218	-101	-29	13	-19	-61	-91	-89	-81	-252	-196	-57
	0,25	-722	-619	-494	-303	-272	-126	-36	17	-24	-76	-112	-112	-103	-311	-245	-70

Table 3. Strain ε for Model C

Direction		Radial direction						Circular direction						Direction at angle of 45°			
														Measured strain ×10⁻⁶			
Strain gauge		1	2	3	4	5	6	7	8	9	10	11	12	13	14	15	16
r / mm		140	145	150	170	180	190	140	145	150	170	180	190	145	150	170	180
Pressure p / MPa	0,05	-163	-144	-122	-42	-22	-9	3	3	4	5	5	7	-72	-58	-18	-8
	0,1	-322	-282	-238	-80	-39	-12	6	5	5	2	2	4	-141	-114	-39	-17
	0,15	-483	-421	-357	-119	-56	-15	8	6	4	-3	-4	-3	-210	-171	-58	-28
	0,2	-646	-565	-478	-160	-74	-17	11	6	3	-7	-13	-12	-282	-231	-78	-40
	0,25	-805	-704	-599	-201	-92	-19	12	7	2	-10	-17	-20	-353	-288	-98	-50

The diagrams of the radial stress for Models A, B, and C, which are obtained using Eq. (2) and Eq. (3) are presented in Figs. 5a, 6a, and 7a, respectively. Figs. 5b and 6b show the displacement diagrams in an axial direction for Models A and B respectively, while Fig. 7b

shows the displacement diagram in a circular direction for Model C.
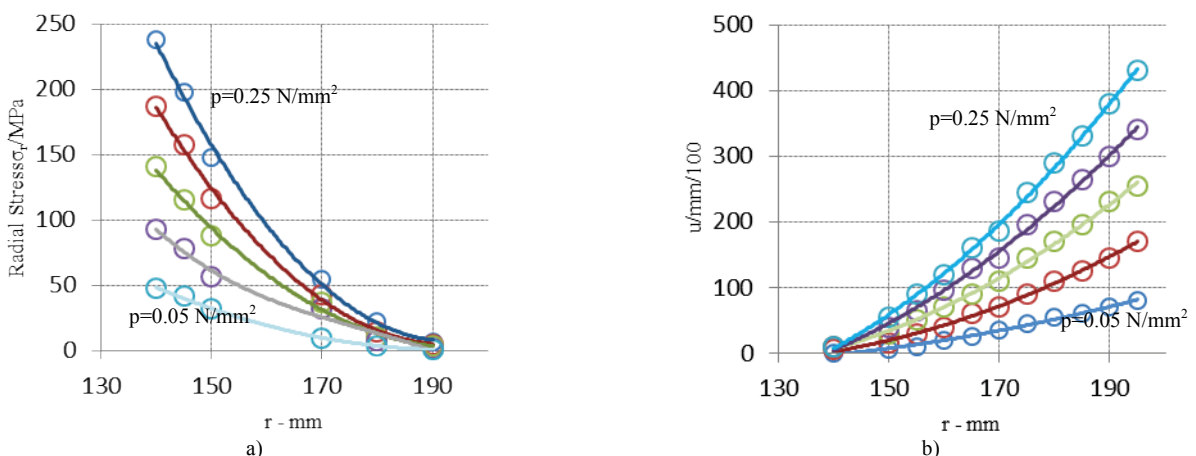
Figure 5 Experimental results for Model A at pressure range 0,05 ÷ 0,25 MPa, given in Tab. 1: a) radial stress, b) displacement in an axial direction
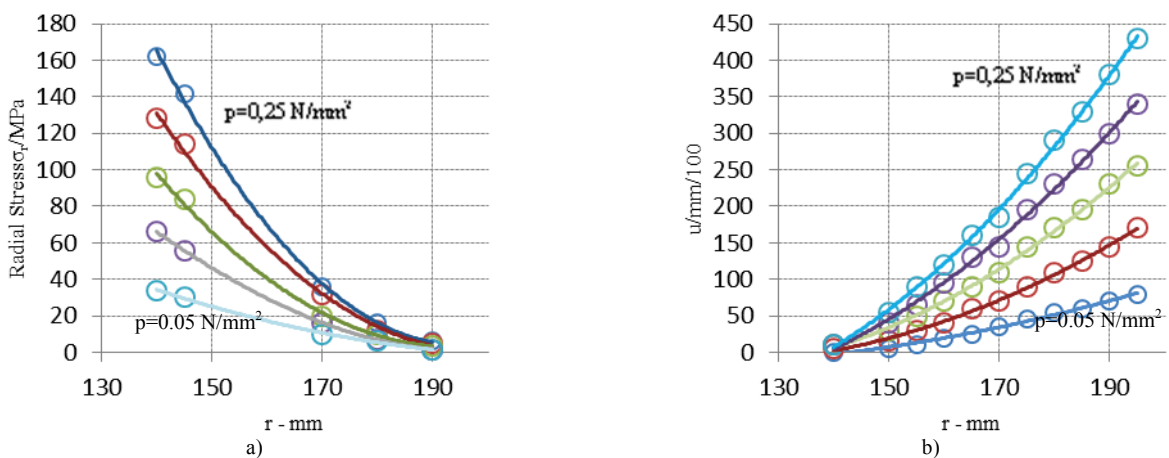

Figure 6 Experimental results for Model B at pressure range 0,05 ÷ 0,25 MPa, given in Tab. 2: a) radial stress, b) displacement in an axial direction
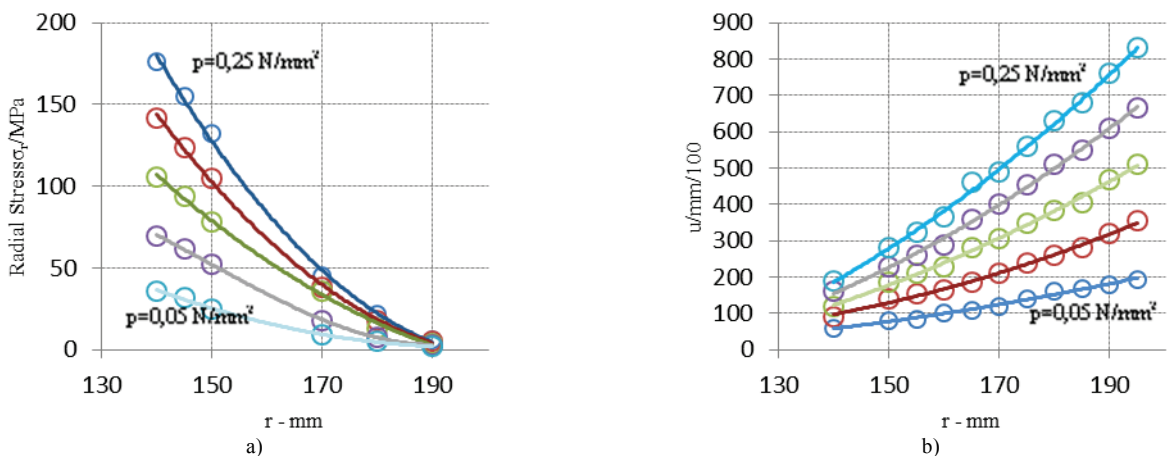

Figure 7 Experimental results for Model C at pressure range 0,05 ÷ 0,25 MPa, given in Tab. 3: a) radial stress, b) displacement in an axial direction

5   Numerical analysis results

Using FEA ANSYS Workbench software with a pre-processor that enables automatic mesh generation for a helicoidal shell on a cylindrical shell, the analyses of Models A, B, and C were performed [16, 17, 18].

In the analysis, structural steel was used as a material for each version, the helicoidal, annular and rectangular shells. The Young's modulus of elasticity value was $E=2\times10^5$ MPa, and Poisson's ratio $\nu=0,3$. The pressure value of $p=0,15$ MPa² was chosen for the analysis.

The fillet at the point $r=130$ mm is made with a radius $\rho=4$ mm, and the software generated a mesh through the whole volume of the cylindrical shell, the joint of the helical and cylindrical shell (fillet) and the helical shell.

5.1 FEA for model A

In Fig. 8a, Model A with constraints and loads is presented. The mesh consists of 13452 elements and 26939 nodes. The distributions of the radial stress for Model A obtained from the FEA are presented in Fig. 8b and 10b.
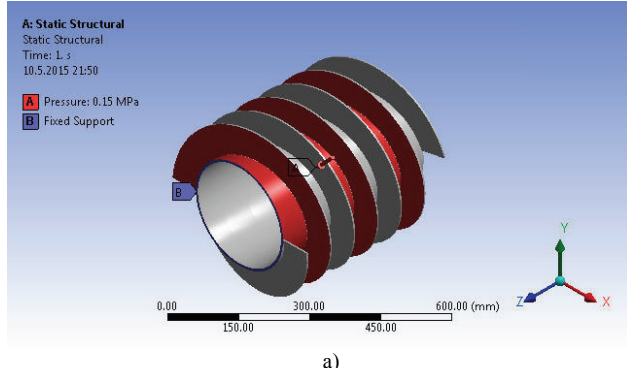
The stress and displacement distribution along the line in the radial direction on the helicoidal shell for Model A is presented in Fig. 9 for the shell thickness h_h=4 mm. The starting point of a 70-mm long interval has the coordinate r=130 mm, while the last point is on the outer helicoidal shell contour and has the coordinate r=200 mm.
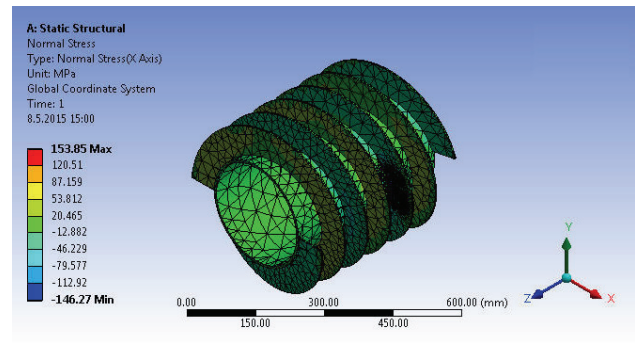
a)   b)

Figure 8 FEA for Model A and the helicoidal shell thickness h_h = 4 mm – a) the Model with loads p=0,15 MPa and constraints, b) distribution of the radial stress
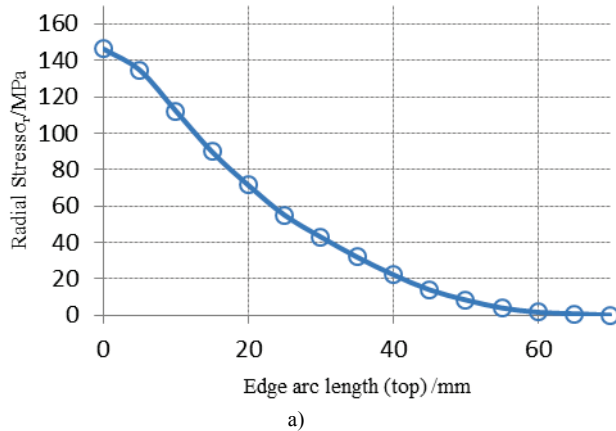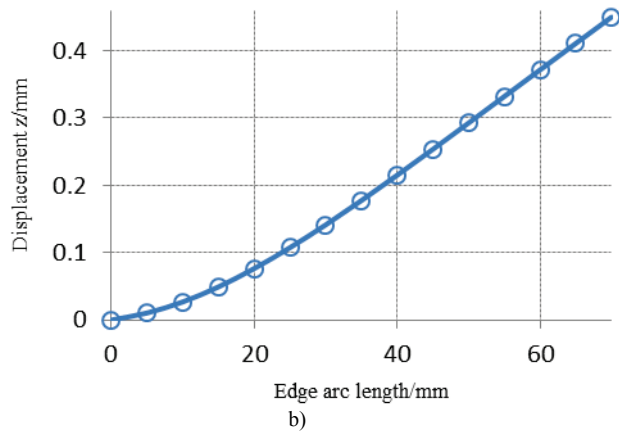

a)   b)

Figure 9 Model A FEA diagrams across the helicoidal shell thickness h_h = 4 mm for a) the radial stress, and b) the displacement in an axial direction

5.2 FEA for Model B

In Fig. 10a, Model B with constraints and loads is presented. The mesh consists of 4575 elements and 9545 nodes. The distribution of the radial stress for Model B obtained from the FEA is presented in Fig. 10b.
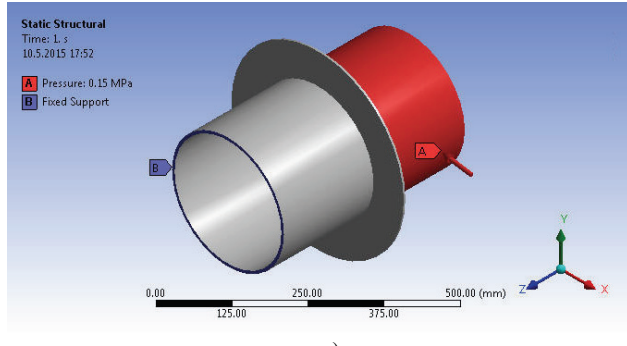
The stress and displacement distribution along the line in a radial direction on the annular shell for Model B is presented in Fig. 11 for the shell thickness h_h=4,15 mm. The starting point of a 70-mm long interval has the coordinate r=130 mm, while the last point is on the outer helicoidal shell contour and has the coordinate r=200 mm.
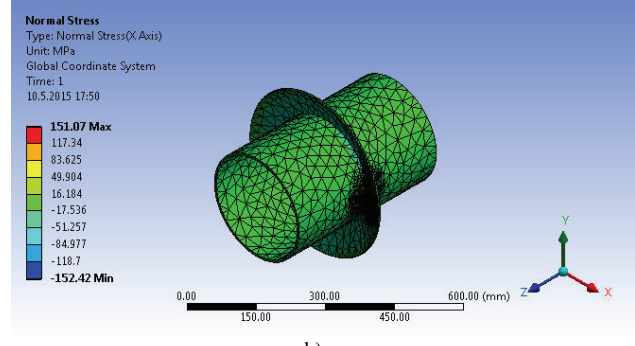

a)   b)

Figure 10 FEA for Model B and the helicoidal shell thickness h_h = 4,15 mm – a) the Model with loads p=0,15 MPa and constraints, b) distribution of the radial stress
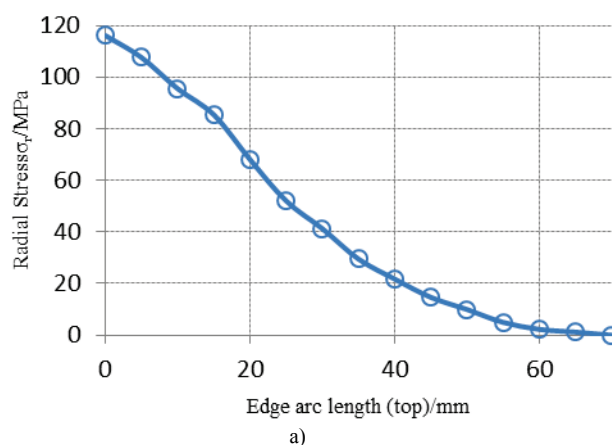
a)
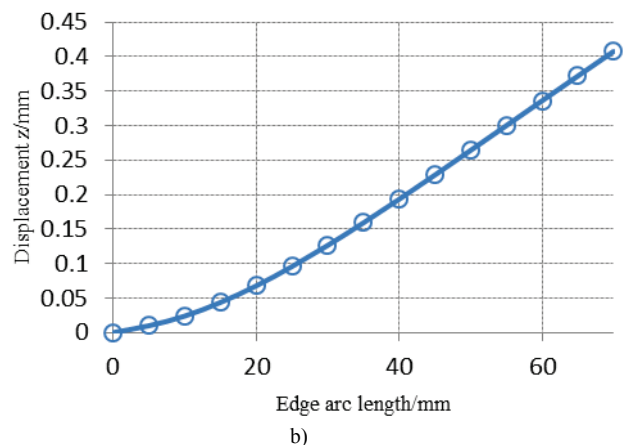
b)

Figure 11 Model *B* FEA diagrams across the helicoidal shell thickness h_h = 4.15 mm for a) the radial stress, and b) the displacement in an axial direction

5.3 FEA for Model C

In Fig. 12a Model C with constraints and loads is presented. The mesh consists of 18212 elements and 35360 nodes. The distribution of the radial stress for Model C obtained from FEA is presented in Fig. 12b.
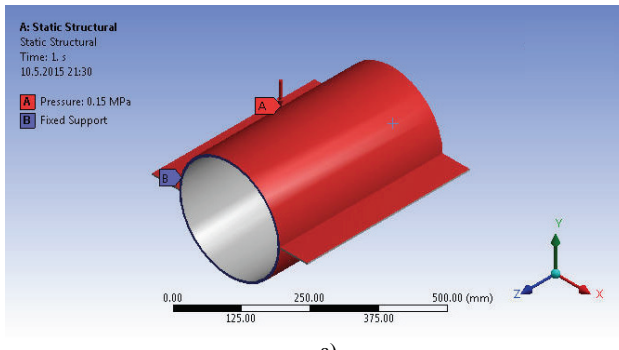

a)
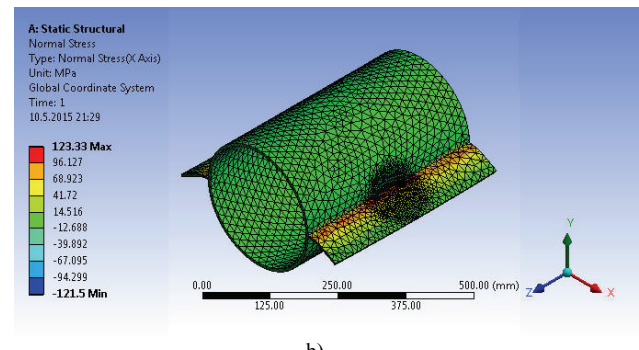
b)

Figure 12 FEA for Model C and the helicoidal shell thickness h_h = 4 mm – a) the Model with loads *p*=0,15 MPa and constraints, b) distribution of the radial stress

The stress and displacement distribution along the line that lies the central plane of rectangular shell and is perpendicular to the cylinder axis is presented in Fig. 13 for the shell thickness h_h=4 mm. The considered interval is 70 mm long with a starting point at the coordinate *r*=130 mm, and an ending point at the coordinate *r*=200 mm.
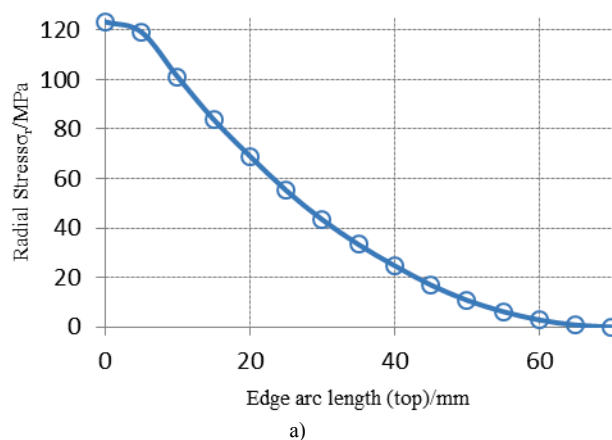

a)
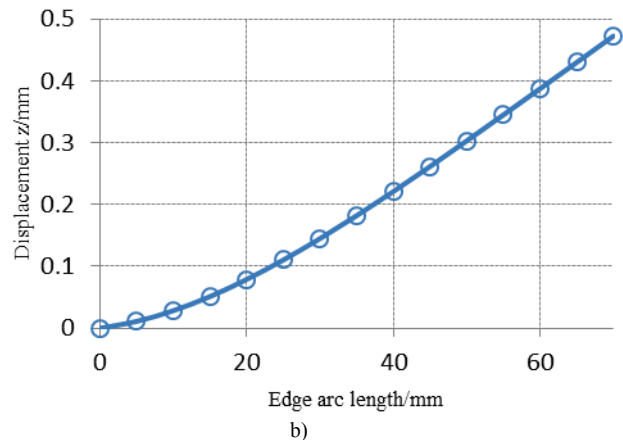
b)

Figure 13 Model *B* FEA diagrams across the helicoidal shell thickness h_h = *4 mm* for a) the radial stress, and b) the displacement in an axial direction

6 Comparison between experimental and numerical results

The diagrams of the stress components distribution obtained from tensometric analysis are in good agreement with the numerical simulation. The results confirm that the radial stress has the maximum stress at the contact zone between the helicoidal and cylindrical shell. Therefore, the geometric parameters of the helicoidal shell can be obtained using limited stress values in that zone as a criterion.

The comparisons of the radial stress σ_r and the circular stress σ_c as well as the displacement for the experimental models *A, B, and C* are given in Tab. 4. The experimental and numerical results show good agreement.

Table 4. Comparative values for stress and displacement for Models A, B and C

| Model | *H*/mm | h_h/mm | Radial stress σ_r/ MPa | | | Displacement *u*/ mm | | |
| | | | *r*=140 mm | | | *r*=195 mm | | |
			Analytic [18]	FEA	Experiment	Analytic [18]	FEA	Experiment
A	140	4	-114,6712	-112,14 (Fig. 9a)	-	-0,4797	0,41099 (Fig. 9b)	-
A	140	3.6	-141,7820	-136,42 (Fig. 11a)	-136,59 (Fig. 5a)	-0,6438	0,54574 (Fig. 10b)	-0,40 (Fig. 5b)
B	0	4,15	-108,3903	-95,519 (Fig. 13a)	-95,93 (Fig. 6a)	-0,3347	0,37188 (Fig. 13b)	-0,26 (Fig. 6b)
C	∞	4	-100,9882	-101,06 (Fig. 15a)	-105,63 (Fig. 7a)	-0,4474	-0,42998 (Fig. 15b)	-0,40 (Fig. 7b)

The discrepancy between the experimental and numerical results for the radial stress is 0,13 %, 0,43 %, and 4,3 % for Models A, B and C, respectively. An experimental investigation of numerous models with a variety of geometric parameters would give better insight into the behavior of the helicoidal shell.

The displacement values obtained from the experiment for Model A (-0,40 mm) and Model B (-0,26 mm) are lower by comparison with the numerical results. This discrepancy might be the consequence of a difference between the real geometric parameters of the experimental model and their nominal values.

The influence of the friction between the special sealing element attached to the helicoidal shell outer edge and the chamber is larger for Model A than for Models B and C. In Models A and B, this friction causes the sign change of the radial displacement at the locations with *r*=190 mm (see Tab. 1 ÷ 3). The influence of friction can be diminished by reducing the surface contact area between the sealing element and the chamber. In addition, the coefficient of friction can be reduced by lubricating and polishing the contact surfaces. The influence of friction in this work can be neglected [14, 18].

Comparable FEA and experimental investigations show that the radial stress is dominant with respect to the circular stress for a helicoidal shell. The highest values of the radial stress are on the joining helical line between the helicoidal and cylindrical shells. These stress values are relevant for the design of machine parts in the shape of the helicoidal shell. The points with the highest stress values are located on the inner part of the helicoidal shell, exactly on the beginning of the fillet that is usually applied to the structures to reduce the stress concentration.

The values of strain in an axial direction measured for experimental model C (Tab. 3.) are negligible. These low values of the strain are a consequence of the small length of the rectangular shells and the fact that in the experimental model their ends were not free after the assembling of the experimental setup. The ends of the rectangular shell were in contact with the cover plates in order to provide for the sealing of the pressurized chamber. Therefore, the ends are loaded in an axial direction. The values of the strain in radial, circular, as well as in the direction of 45° with respect to the radial direction are measured at the shell points with the same *r* coordinate. The comparison of these values shows that the main stress directions are close to the radial and axial directions, which is confirmed by the main stress diagrams derived from the numerical analyses [13, 19].

7 Conclusion

The investigation presented in this paper is part of a wider examination of elements of helicoidal shells, for which a range of theoretical, experimental and mathmatical approaches are used.

This paper presents original experimental and numerical approaches. A close match between the results from experimental analyses and calculations by finite elements method was demonstrated. The results obtained show that by designing twin helicoidal shell and using the suggested sealing method on the long contact length, where pressure in the chamber is simultaneously used for better seal adherence, it is possible to investigate the different regimes of the helicoidal shell.

For example, the radial stress results closely agree with the model results, where the discrepancy is 0,13 %, 0,43 % and 4,3 % for Models A, B and C respectively. If you compare the results from the previously presented theoretical analysis, you find a discrepancy in the maximum and minimum values of the radial displacement of 3,78 %, 11,87 % and 4,39 % for Models A, B and C respectively. Given the complexity of the process and the great number of variable parameters (friction, exactness of dimensions, the anistropy and so on) we can here speak of a very good result.

In terms of the displacement, given the low values, the relative indicators are not a good basis for the successful measurement of performance. It is clear that the changes in the sign of the displacement indicate that there is a need for the adaptation of the software used to the needs of this area of research. In experimental research, it has been shown that the directions of the principal stresses are very close to the radial and circular directions. The strains in an axial direction for a rectangular shell are lower than the ones in a circular direction for an annular shell and helicoidal shell.

The presented approach can be completely applied to an experimental research of helicoidal shells of variable thickness. This approach opens the possibilities for the experimental research of the shells in the shape of a conoidal surface whose generetrixes need not be parallel to the *Oxy* plane as well as for the research of other shapes of conoidal surfaces.

In further investigations, it is possible to work on the development of an approach for the experimental research of a helicoidal shell exposed to a tangent load on its own surface.

Nomenclature

H − pace of helical line, mm
$D, d, h, b, \delta_1, \delta_2$ − shell geometric parameters, mm
k − shell inclination, mm
p − pressure, MPa
r, φ − polar coordinates, mm, °
μ − strain coefficient for tensometric measurements, -
$\varepsilon_1, \varepsilon_2$ − main strains, -
σ_1, σ_2 − main stresses, MPa
σ_r, σ_c − radial and circular stress and axial direction, MPa
E − elastic modulus, MPa
ν − Poisson's ratio, -
u – displacement, mm

Acknowledgments

8 References

[1] Gol'dveizer, A. L. The Role of Surface Bendings in the Shell Theory. // Symposium on Shell Theory, Proceedings of the Third IUTAM/ Tbilisi, 1978, pp.315-323.
[2] Timoshenko, S.; Woinowsky–Krieger, S. Theory of plates and shells. McGraw – Hill Book Company Inc., 1987.
[3] Naghdi, P. M. The Theory of Shells and Plates, Mechanics of Solids. Springer-Verlag, Berlin, 1984.
[4] Феодосеев, В. И. Сопротивление материалов. Наука, Москва, 1973.
[5] Wlassow, W. S. Allgemeine Schalentheorie und ihre Anwendung in der Technik. Akademie-Verlag, Berlin, 1958.
[6] Novozhilov, V. V. The Theory of Thin Shells (translation from 1951. Russian edition). Noordhoof, Groningen, 1959.
[7] Krivoshapko, S. N.; Gerard, G. A. Two methods of analysis of thin elastic open helicoidal shells. // IJRRAS, 12, 3(2012), pp. 382-390.
[8] Krivoshapko, S. N.; Bock Hyeng, C. A. Static and Dynamic Analysis of Thin-Walled Cyclic Shells. // International Journal of Modern Engineering Research (IJMER), 2, 5(2012), pp. 3502-3508.
[9] Merlini, T.; Morandini, M. Helicoidal Shell Theory. // DIA-SR 08,07(2008)
[10] Cohen, J. W. On Stress Calculations in Helicoidal Shells and Propeller Blades. Waltman, Delft, 1955.
[11] Cohen, J. W. The Inadequacy of the Classical Stress-Strain Relations for the Right Helicoidal Shell. // Theory of Thin Elastic Shells, Proceedings of the Symposium/ North-Holland, Delft, 1959, pp. 415-433.
[12] Mikhlin, S. G. Estimate of the Error in the Computation of an Elastic Shell as a Flat Plate. // Akademija nauka SSSR, Prikladnaja matematika 16/ Moskva, 1952.
[13] Love, A. E. H. A treatise on the mathematical theory of elasticity I and II. Cambridge, 1927.
[14] Savićević, S. A Development of Automatized Projection of Construction Elements of Helical Shell Shape. // PhD dissertation, Faculty of Mechanical Engineering / Podgorica, 2001.
[15] Savićević, S.; Đogović, V. Bending of Structural Elements of the Helicoidal Shell Shape. // Theoretical and Applied Mechanics, Proceedings of 23rd Yugoslav Congress, 1999.
[16] Merlini, T.; Morandini, M. Computational shell mechanics by helicoidal modeling II: Shell element. // Journal of Mechanics of Materials and Structures, 6, 5(2011). DOI: 10.2140/jomms.2011.6.693
[17] Sadowski, A. J.; Rotter, M. J.; On the relationship between mesh and stress field orientations in linear stability analyses of thin plates and shells. // Finite Elements in Analysis and Design, 73,C(2013), pp. 42-54. DOI: 10.1016/j.finel.2013.05.004
[18] Savićević, S.; Zeković, S. Analysis of machine elements in shape of helicoidal shell on cylindrical shell. // Proceedings of the Institution of Mechanical Engineers, Part C: Journal of Mechanical Engineering Science, 221, C6(2007), pp. 627-638. DOI: 10.1243/0954406JMES481
[19] Shevelev, L. P.; Korikhin, N. V.; Golovin, A. I. Field stress state in the helicoidal shell. // Stroitel'stvo Unikal'nyh Zdanij i Sooruzenij, 2, (2014), pp. 25-38.

Authors' addresses

Sreten Savićević, PhD, Associate Professor
University of Montenegro – Faculty of Mechanical Engineering
Cetinjska 2, 81 000 Podgorica, Montenegro
sreto@ac.me

Željko Ivandić, PhD, Full Professor
Mechanical Engineering Faculty
Trg Ivane Brlić Mažuranić 2
Slavonski Brod, HR-35000, Croatia
Zeljko.Ivandic@sfsb.hr

Janko Jovanović, PhD, Associate Professor
University of Montenegro – Faculty of Mechanical Engineering
Cetinjska 2, 81 000 Podgorica, Montenegro
janko@ac.me

Luka Grubiša, BsC
University of Montenegro – Faculty of Mechanical Engineering
Cetinjska 2, 81 000 Podgorica, Montenegro
luka.grubisa@yahoo.com

Antun Stoić, PhD, Full Professor
Mechanical Engineering Faculty
Trg Ivane Brlić Mažuranić 2
Slavonski Brod, HR-35000, Croatia
Antun.Stoić@sfsb.hr

Milan Vukčević, PhD, Full Professor
University of Montenegro – Faculty of Mechanical Engineering
Cetinjska 2, 81 000 Podgorica, Montenegro
milanvu@ac.me

Mileta Janjić, PhD, Associate Professor
University of Montenegro – Faculty of Mechanical Engineering
Cetinjska 2, 81 000 Podgorica, Montenegro
mileta@ac.me